THE JOURNAL OF PHYSICAL CHEMISTRY LETTERS
A JOURNAL OF THE AMERICAN CHEMICAL SOCIETY

pubs.acs.org/JPCL

Letter

Optical Cycling Functionalization of Arenes

Claire E. Dickerson, Han Guo, Guo-Zhu Zhu, Eric R. Hudson, Justin R. Caram, Wesley C. Campbell, and Anastassia N. Alexandrova*

Cite This: *J. Phys. Chem. Lett.* 2021, 12, 3989−3995

Read Online

ACCESS | Metrics & More | Article Recommendations | Supporting Information

ABSTRACT: Closed, laser-induced optical transitions ("optical cycling transitions") of molecules can be used for state preparation and measurement in quantum information science and quantum sensing. Increasingly complex molecular species supporting optical cycling can provide new capabilities for quantum science, and it is not clear if there is a limit on their size or complexity. We explore Ca−O−L molecular constructs to support the optical cycling center, Ca, with ligands, L, being arenes. We find that L can be as large as coronene (i.e., $CaOC_{24}H_{11}$) without losing the diagonality of the Franck−Condon factor (FCF). Furthermore, L can be substituted with electron-withdrawing groups to improve the FCF. Larger L, beyond ∼7 rings, can disrupt the diagonality of the FCF by closing the HOMO−LUMO ligand electronic state gap and reordering with the local states on the cycling center. Overall, we find that optical cycling can be retained for arenes, and we offer a principle for their design.

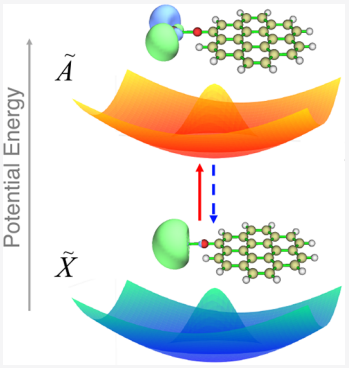

Experimental quantum information science is built on systems that feature easily prepared and measured quantum states, such as spin states, for utilization as qubits. Currently, superconducting qubits and trapped atomic species arguably lead this quantum hardware race. Atoms and atom-like molecular moieties with optically induced, closed transitions have been explored in the field of atomic physics, particularly in the context of laser cooling, for quantum computation, analog quantum simulation, and precision measurement.[1−5] Alkaline earth and, recently, other metals, ionically bonded to an oxygen linearly bonded to an R-group ligand (M−O−R) were shown to be capable of optical cycling, such as SrOH, CaOH, BaOH, and, most recently, YbOH.[6−10] Additionally, symmetric top molecules, such as $CaOCH_3$, $SrOCH_3$, $BaOCH_3$, and $YbOCH_3$, were shown to be optical cycling centers (OCCs).[11−18]

Even larger molecules, such as calcium phenoxides, have been proposed as M−O−R OCCs theoretically.[19,20] Recently, an extension of such OCCs toward larger polyatomic molecules has been realized in the laboratory. It is currently an open question of whether the optical cycling of functionalized molecules can be engineered so that the Franck−Condon factor (FCF) can be retained in the large-molecule limit (i.e., where the molecular ligand grows beyond a size where its details no longer affect the optical cycling). Should this prove possible, it would open the door to adding a modularized quantum state readout to any substrate to which such a ligand can be attached.

In this Letter, we show that the ligand, L, in Ca−O−L can grow beyond a single carbon ring to larger arenes. This is possible because the geometries of arenes are relatively rigid and their electronic states feature substantial gaps in their highest occupied molecular orbital (HOMO) to their lowest unoccupied molecular orbital (LUMO), which do not mix with the states on Ca because they belong to a different irreducible representation in the C_s or C_{2v} point group. The energies of the electronic states of arenes are also easily tuned by electron-withdrawing substitutions on the ring and by arene size.

Conveniently for this investigation, arenes are abundant throughout the universe[21−24] and extensively characterized by, for example, infrared (IR) spectroscopy.[25] Databases exist containing vibrational harmonic spectra for arenes, namely, polycyclic aromatic hydrocarbons, up to hundreds of carbon atoms.[26,27] Thus, the extension toward the application of arenes in optical cycling benefits from both existing insights from laser cooling molecules and a knowledge of extensive arene IR vibrational spectra. Thus, much of the groundwork necessary for adding OCCs to arenes for quantum measurement and computing is already in place.

Previously, identifying optically cyclable molecules required either finding spectrocopic properties (such as diagonal FCFs) in the literature or through trial and error. However, recently, some design strategies have emerged. Ivanov et al. showed that an alkaline earth metal radical can be attached to a phenyl group, cyclopentadienyl, and pyrrolide and that the metal could retain some optical cycling capabilities.[19] Additionally,

Received: March 5, 2021
Accepted: April 12, 2021
Published: April 20, 2021

https://doi.org/10.1021/acs.jpclett.1c00733
J. Phys. Chem. Lett. 2021, 12, 3989−3995

they showed that multiple optical cycling radicals could be attached to the same ligand if they are sufficiently spaced.[28] In a recent study, we showed that a cycling Ca or Sr radical attached to a phenoxide can have its diagonal FCF boosted by chemical substitution on the far side of the carbon ring.[20] For an electronic transition isolated on a metal radical, the FCF is boosted in a manner that can be predicted by the sum of the substiuents' Hammett parameters. Specifically, electron-withdrawing groups spatially isolated from the cycling center increase the diagonality of the FCF by creating more similar ground- and excited-state potential energy surfaces, where the largest off-diagonal decay is the Ca−O stretching mode.

This earlier work led us to realize that the ligand HOMO−LUMO gap might play an important role in keeping the electronic states of the cycling center and the associated transition isolated. Here, we hypothesize that the HOMO−LUMO gap is one of the key design parameters for larger molecules that can support optical cycling centers with diagonal FCFs. We explore this possibility on the basis of the Ca−O−L platform, where L is an arene. Arenes are rigid molecules, so their HOMO−LUMO gap can be reliably modified via the number of conjugated aromatic rings. Therefore, we explore arene ligands of increasing size, from naphthalene to ovalene, as well as the large ligand limit simulated by a graphene edge. In this way, we expose the L's HOMO−LUMO gap as an important design consideration for expanding the repertoire of L for optical cycling. We additionally explore the relative orientation of L and Ca (or Ca−O placement on the arene rings) as well as the further functionalization of arenes with fluorines. All studied molecular ligands are shown in Figure 1, while a 2D graphene material ligand is discussed later in Figure 6.

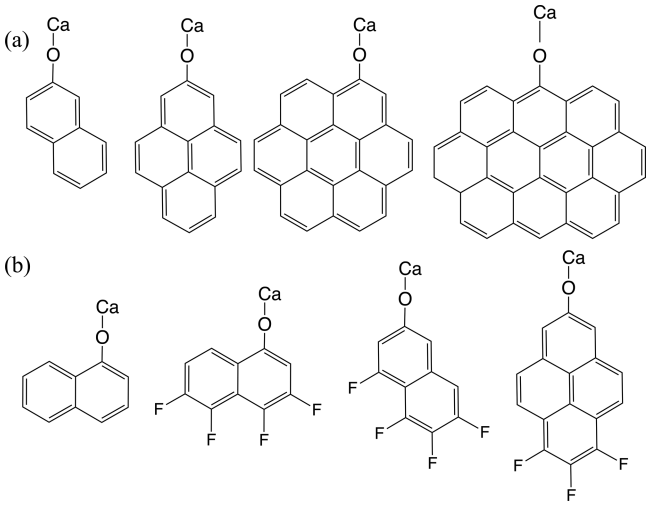

Figure 1. Arenes decorated with optical cycling motifs that are considered in this study. Row a, left to right: naphthalene, pyrene, coronene, ovalene. Row b, left to right: h-naphthalene ("h" stands for "horizontal") and fluorinated derivatives (F-h-naphthalene, F-naphtalene, and F-pyrene).

For a species to host an optical cycling transition, the first electronic excitation must be exceptionally vertical and feature minimal vibrational leakage channels for nonradiative decay. The transition should also be isolated from other excitations and lie below the dissociation threshold. Previous calculations and experiments identified the existence of low-lying excited states for CaL complexes.[6−9] For the CaO−arenes with C_s symmetry, the A′′ state lies close in energy to the A′ state examined in this work. Our calculations in Table S2 suggest that the A′′ and A′ states have small energy splitting but are not degenerate, with the magnitude of the splitting similar to that found in CaOPh.[20] There is a possibility that these states cross via out-of-plane vibrations, in which case DFT is no longer a sufficient approach, whereas multireference approaches are very expensive for systems of this size. Hence, it will be important to verify experimentally that the A′ and A′′ states do not reorder. For the vertical transition, it is advantageous for both the ground- and excited-state electron densities to be localized on the cycling center (in this work, the Ca radical) in Ca−O−L and feature a minimal (and equal) amount of Ca−O bond covalency. The natural transition orbitals (NTOs) of the HOMO ($\tilde{X}$) to LUMO ($\tilde{A}$) transition for CaO−naphthalene and CaO−coronene are shown in Figure 2. The electron density remains isolated on the metal,

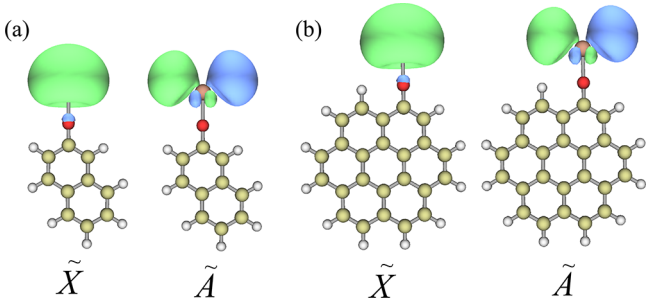

Figure 2. CaO-functionalized naphthalene and coronene NTOs of the ground- to first excited-state transition ($\tilde{X} \rightarrow \tilde{A}$) with an isosurface value of 0.03. No wavefunction can be found far from the calcium.

with a very small contribution from the oxygen. The Ca−O bond ionicity is confirmed for the ground states via natural population analysis (NPA) (Table 1). These results suggest that all molecules feature highly ionic Ca−O bonds, and the ionicity increases slightly upon fluorination.

Table 1. Computed NPA Charges on Ca and O for All CaO−Arenes' GroundStates

substituent	charge (Ca)	charge (O)
benzene	0.95672[20]	−1.06673[20]
naphthalene	0.95817	−1.06100
pyrene	0.95924	−1.06000
coronene	0.96138	−1.04898
ovalene	0.96578	−1.03405
h-naphthalene	0.96077	−1.05630
F-h-naphthalene	0.96053	−1.03787
F-naphthalene	0.96086	−1.04382
F-pyrene	1.00522	−1.09231

Next, we explore the similarity between the ground and first excited electronic potential energy surfaces (Table 2). The Ca−O bond length changes between the minimum on the ground-state surface and the minimum on the excited-state surface are below 0.02 Å for all considered species. The bond-length change becomes smaller upon fluorination, consistent with the increasingly isolated character of the radical and in accordance with the design principle introduced in ref 20. Also, we find that the placement of the O−Ca moiety on the arene

https://doi.org/10.1021/acs.jpclett.1c00733
J. Phys. Chem. Lett. 2021, 12, 3989−3995

Table 2. FCFs and Ca−O Bond Length Change (Excited State − Ground State) for All Molecules

substituent	FCF	Ca−O change (Å)
benzene	0.958[20]	−0.0168[20]
naphthalene	0.958	−0.0163
pyrene	0.947	0.0164
coronene	0.931	−0.0140
ovalene	0.167	−0.0010
h-naphthalene	0.931	−0.0163
F-h-naphthalene	0.917	−0.0133
F-naphthalene	0.968	−0.0127
F-pyrene	0.962	−0.0151

plays an important role, as the horizontal derivatives have larger differences between the ground and the excited potential energy surfaces.

Although the unpaired electron is localized on the metal throughout the transition, there is a nearly linear decrease in FCF as the arene ligand increases in size from naphthalene to coronene. The decrease can be related to the slight decrease in the isolated character of the frontier orbitals on the cycling molecules (Figure 3). As the arene gets larger, its intrinsic

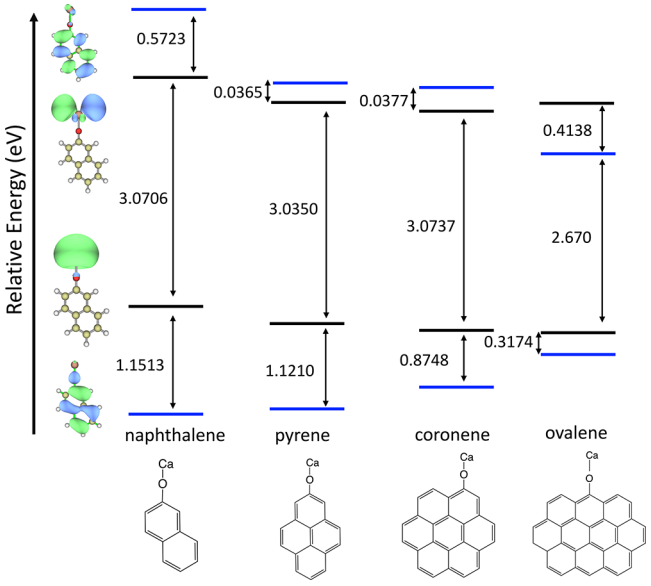

Figure 3. DFT energies of electron density localized on the ligand (the ligand HOMO−LUMO gap (blue)) and density localized on the metal (metal HOMO−LUMO gap (black)) for CaO−naphthalene, CaO−pyrene, CaO−coronene, and CaO−ovalene. As the ligand size increases, the ligand HOMO−LUMO gap decreases and approaches the isolated metal−metal electronic transition until the transition is disrupted by the switching of the metal and ligand LUMOs, as seen in CaO−ovalene.

HOMO−LUMO gap (which, for example, in CaO−pyrene corresponds to the HOMO − 1 to LUMO + 1 gap, shown in blue in Figure 3) closes and approaches the metal-based electronic transition (shown in black in Figure 3). The ligand and Ca lowest unoccupied orbitals become particularly close as the arene increases in size. While FCFs can be improved slightly by substituting electron-withdrawing groups on the ligand, once L becomes ovalene, the verticality of the transition is lost due to the excited-state order switch, whereby the LUMO becomes an arene-centered orbital, as seen in Figure 3. Fluorinating these species systematically shifted all energy levels lower in energy, but the relative HOMO−LUMO gaps remained similar to their unsubstituted versions (Supporting Information). Although bond length is a good indicator of FCF when adding electron-withdrawing groups, CaO−arenes, which have varying ligand HOMO−LUMO gap sizes that can interact with the metal, affect the FCF more than just the bond-length change because the closer the ligand HOMO−LUMO gap is to the metal HOMO−LUMO gap, the more dominant other vibrational leakage pathways, such as in-plane bending, become.

The HOMO−LUMO gap of the "ligands", where the electron density is not on the metal but solely on the arene molecule, is shifted but still close to the experimental electronic excitation energies of their singlet, neutral counterparts. These neutral species' electronic excitations were also benchmarked against experiment,[29−31] using our computational methodology (Supporting Information).

From a vibrational mode perspective, the dominant off-diagonal decay mode changes depending on the arene size and symmetry (Figure 4). In CaO−naphthalene, the first two off-

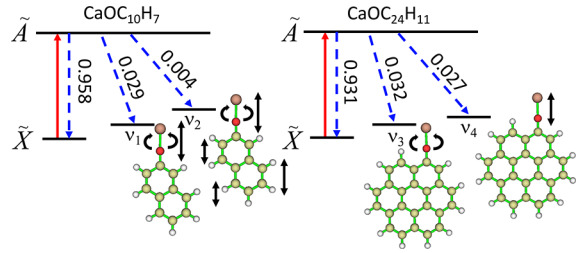

Figure 4. Photon cycling scheme with an excitation (red) to the first excited electronic state and decay (blue) to the ground electronic state for CaO−naphthalene and CaO−coronene. The FCFs are shown along with each decay pathway.

diagonal modes are the symmetric Ca−O stretch and a Ca−O bend and stretch. However, with coronene, the dominant off-diagonal mode is the Ca−O in-plane bending, followed by the Ca−O symmetric stretch. This could be due to the interaction of the unpaired electron on Ca with the delocalized electronic states on the arene; these states have a greater spatial overlap in the horizontal variants and better match in energy with larger arenes. For the same reason, we also conclude that placing the cycling center on a C_6 ring that is more isolated from the rest of the polyaromatic system of the arene helps diagonalize the FCF.

Besides the vibrational losses due to the off-diagonal vibrational modes, rotational branching can cause leakage of the closed optical cycling. With low symmetries like C_s, the functionalized arenes are asymmetric top molecules possessing complex rotational structures, which make it challenging for optical cycling. As discussed previously,[15,32] however, carefully chosen rotational transitions following specific rotational and parity selection rules can limit or eliminate the rotational losses.

The FCF decrease can be mitigated slightly by adding electron-withdrawing groups at positions on the arenes such that the Ca−O symmetric stretch behavior is favored (i.e., far away from Ca−O) (Table 2 and Figure 5). The substituted F versions of the molecules designed in this way have more similar ground- and excited-state potential energy surfaces and thus larger FCFs than unsusbtituted arenes.

https://doi.org/10.1021/acs.jpclett.1c00733
J. Phys. Chem. Lett. 2021, 12, 3989−3995

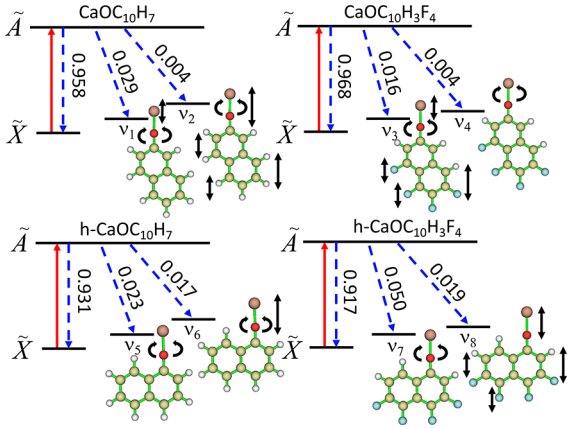

Figure 5. Photon cycling scheme with an excitation (red) to the first excited electronic state and decay (blue) to the ground electronic state for, from left to right, CaO−naphthalene, CaO−F−naphthalene, CaO−h-naphthalene, and CaO−F−h-naphthalene. The FCFs are shown along with each decay.

Intriguingly, we find that for the horizontal arene ligands, where the in-plane bending mode is already the dominant vibrational leakage channel, fluorination does not help diagonalize the FCF (Table 2 and Figure 5). When fluorines are substituted, FCFs decrease, and the bend's off-diagonal decay increases to 0.05. Therefore, the vertical arene ligands are more favorable than the horizontal arene ligands for optical cycling.

Since increasing arene ligand size appears to lead to the eventual destruction of diagonal FCFs, we pushed the concept to its limit and examined Ca−O bound to the edge of 2D graphene. We consider two edge structures (Figure 6): in E1, Ca−O−C maintains a locally linear structure in the ground electronic state, while in E2, Ca−O−C is bent at an angle of 163.9° due to the asymmetrical local structure and charge density.

In the density of states (DOS) calculations, we see density mixing on graphene and the metal, for both structures, and for both the ground and excited states. This disrupts the clean transitions, leading to poor FCFs. This is further illustrated by the plots of the charge density, showing the lack of localization and the spread of the charge density throughout the graphene edge. The orbitals of Ca mix with C orbitals and split into two mixed orbitals. Thus, while functionalization of large-band-gap diamond with M−O optical cycling centers was proposed to be possible,[33] the graphene edge is not a suitable substrate for this purpose. This is explained by the ligand band gap paradigm proposed in this work.

Finally, how could one synthesize such large molecules as arenes functionalized with optical cycling centers? Experimentally, various methods have been developed to produce the alkaline earth radical-containing molecules via reactions of the metal atoms with the volatile ligands.[15,16,34] The metal atoms are generated either by evaporation in a Broida-type oven[34] or by laser ablation of the metal targets. The atoms then react with the gaseous precursors to form the products. The reaction rate is likely enhanced when pumping the ground-state metal atoms to the metastable excited states.

Supersonic jet and cryogenic buffer-gas cooling[15,16] are commonly employed to make products vibrationally and rotationally cold. The functionalized arenes discussed here can be produced using a similar method. Take CaO−naphthalene

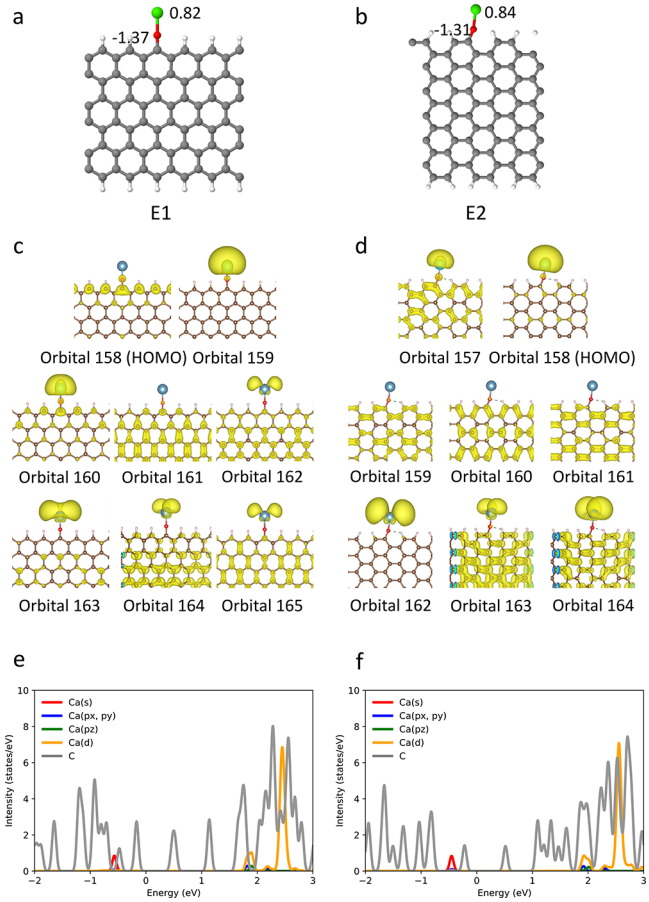

Figure 6. (a and b) Optimized ground-state structures for two edge structures, E1 and E2. The atomic charges on Ca and O from the Bader charge analysis are also shown. (c and d) Electron density of molecular orbitals for CaO supported on two graphene edges. The isosurfaces are plotted with an isovalue of 0.001. (e and f) PDOS for CaO supported on two graphene edges.

as an example: a nanosecond 1064 nm Nd:YAG laser is used to ablate the calcium target, producing Ca atoms. Since the ligand, 2-naphthol, is involatile and has a melting point of around 120 °C, a heated source is used to melt the 2-naphthol to generate enough vapor, which is entrained in a cryogenic buffer gas of helium to react with Ca atoms. The formed CaO−naphthalene can be probed by laser spectroscopy. At cryogenic temperature, clustering could be possible between the helium gas and molecules with binding energies of around 100 cm^{-1},[35] which may impede reaction efficiency. However, previous buffer gas cooling experiments, including naphthalene ($C_{10}H_8$),[36] *trans*-stilbene ($C_{14}H_{12}$), and Nile red ($C_{20}H_{18}N_2O_2$),[35] showed no evidence of forming helium-molecule clusters at a cold temperature, of around 7 K, though an upper limit of 5% is estimated for the population of the He-*trans*-stilbene cluster. This is likely due to the low number density of helium (typically around 10^{14} cm^{-3}) under the buffer gas condition. The arenes studied here are of similar size to the species in these studies and so likely will not cluster with He to affect the reaction efficiency with the ablated metal atoms.

To conclude, in this work it was found that arene ligands attached to a linear Ca−O could be suitable for optical cycling. We propose a design strategy and a way to foresee the limit on the molecular size permitting the preservation of optical

https://doi.org/10.1021/acs.jpclett.1c00733
J. Phys. Chem. Lett. 2021, 12, 3989−3995

cycling. The cycling functionality of these large molecules is dependent on the size of the arene and its orientation with respect to the Ca−O center. As the arene ligand grows, its intrinsic HOMO−LUMO gap becomes smaller which encourages vibrational mode mixing and electronic state reordering of the ligand and cycling center. These effects produce greater differences between the ground- and excited-state potential energy surfaces and less diagonal FCFs. Extending arenes all the way to ovalene or graphene destroyed the clean electronic transition in this way, as the graphene edge states mixed with the electronic transition in CaO−graphene and the ligand LUMO switched with the metal LUMO in CaO−ovalene. An arene as large as coronene is predicted to be a successful host for the Ca−O OCC, being the largest such ligand proposed to date.

An extension to ligands of similar size is an ongoing investigation. Molecules that fail as OCC ligands will be flexible and allow the Ca−O bond and ligands to bend/rotate, such as long chains of saturated hydrocarbons, and have strong electron-withdrawing groups close to the metal, reactive unsaturated hydrocarbons not in a ring close to the metal, or small HOMO−LUMO gaps. Small arene molecules work well as OCC ligands due to their large HOMO−LUMO gap, planar, rigid structure, and low reactivity with the metal, but eventually the clean electronic transition will be disrupted if the molecule grows too large. Alternatively, a material that can be grown large and support an OCC is diamond because it has a large band gap and is quite rigid so that it does not interact with the OCC.[33]

COMPUTATIONAL METHODS

All molecules were calculated at the PBE0-D3/def2-TZVPPD level of theory[37−39] with DFT and time-dependent density functional theory (TD-DFT) on a superfine grid using *Gaussian 16*.[40] This level of theory was previously extensively benchmarked against multireference CAS-PT2 calculations for CaOH, SrOH, CaF, SrF, and $CaOCH_3$.[20] Additionally, electronic excitation energies for neutral naphthalene, pyrene, and coronene, computed with TD-DFT matched experimental data within 0.04 eV (Supporting Information). FCFs, including Duschinsky rotations, were calculated from harmonic vibrational frequencies. The harmonic approximation is expected to be reliable because the optical center is well-isolated from the modes of the ligand and the anharmonicity, if any, will be similar from the ground state to the excited state and should not affect the diagonality of the FCF, as we detailed previously for calcium phenoxides.[20] Also, for naphthalene, anthracene, and tetracene, the main anharmonic modes were the C−C or C−H stretches in the 1300−1600 cm^{-1} range[41,42] (i.e., sufficiently far from Ca−O stretching or bending modes (dominant contributors to the FCF which are less than 700 cm^{-1}). However, a discussion of anharmonic effects is included in the Supporting Information. Additionally, rotational losses are outside the scope of this Letter, but a discussion of asymmetric tops and rotational losses can be found in Augenbraun et al.[32] Multiwfn was used for molecular visualizations.[43]

OCCs bound to the edge of single-layer graphene were computed using VASP.[44−47] Geometry optimizations were carried out using PBE.[48,49] The hybrid functional, HSE06, was used for the charge density and density of states calculations[50−52] because it has been previously benchmarked against experiment for the prediction of band gaps.[53,54] The interactions between the ionic cores and the electrons were described using the projector augmented wave (PAW) potentials.[55,56] A 1 × 4 × 1 Monkhorst−Pack k-point grid and a plane wave cutoff energy of 400 eV were employed. The 2D graphene sheet was represented as an infinite strap with periodic boundary conditions, in which the two edges were covered with H atoms, one of which was removed to deposit CaO. We used a large unit cell of 15 Å × 15 Å × 25 Å to prevent the interaction between periodic images. The top three layers of C atoms and the top-edge H atoms were relaxed during the geometry optimization, with a convergence criterion of 0.01 eV/atom.

ASSOCIATED CONTENT

Supporting Information

The Supporting Information is available free of charge at https://pubs.acs.org/doi/10.1021/acs.jpclett.1c00733.

Energy-level diagrams for fluorinated arenes and horizontal naphthalene; TD-DFT benchmarking for neutral, singlet arene species; TD-DFT of A′ and A″ states for C_s-symmetry molecules; and additional FCF effects (anharmonicity, Duschinsky rotations) (PDF)

AUTHOR INFORMATION

Corresponding Author

Anastassia N. Alexandrova − *Department of Chemistry and Biochemistry, University of California, Los Angeles, California 90095, United States;* orcid.org/0000-0002-3003-1911; Email: ana@chem.ucla.edu

Authors

Claire E. Dickerson − *Department of Chemistry and Biochemistry, University of California, Los Angeles, California 90095, United States*

Han Guo − *Department of Chemistry and Biochemistry, University of California, Los Angeles, California 90095, United States;* orcid.org/0000-0001-7695-9080

Guo-Zhu Zhu − *Department of Physics and Astronomy, University of California, Los Angeles, California 90095, United States*

Eric R. Hudson − *Department of Physics and Astronomy, University of California, Los Angeles, California 90095, United States*

Justin R. Caram − *Department of Chemistry and Biochemistry, University of California, Los Angeles, California 90095, United States;* orcid.org/0000-0001-5126-3829

Wesley C. Campbell − *Department of Physics and Astronomy, University of California, Los Angeles, California 90095, United States*

Complete contact information is available at: https://pubs.acs.org/10.1021/acs.jpclett.1c00733

Notes

The authors declare no competing financial interest.

ACKNOWLEDGMENTS

This work was supported by the U.S. Department of Energy, Office of Science, Basic Energy Sciences, under award no. DE-SC0019245. Computational resources were provided by XSEDE.

REFERENCES

(1) Shuman, E. S.; Barry, J. F.; Glenn, D. R.; DeMille, D. Radiative Force from Optical Cycling on a Diatomic Molecule. *Phys. Rev. Lett.* **2009**, *103*, 223001.

(2) Hummon, M. T.; Yeo, M.; Stuhl, B. K.; Collopy, A. L.; Xia, Y.; Ye, J. 2D Magneto-Optical Trapping of Diatomic Molecules. *Phys. Rev. Lett.* **2013**, *110*, 143001.

(3) Truppe, S.; Williams, H. J.; Hambach, M.; Caldwell, L.; Fitch, N. J.; Hinds, E. A.; Sauer, B. E.; Tarbutt, M. R. Molecules Cooled below the Doppler Limit. *Nat. Phys.* **2017**, *13*, 1173−1176.

(4) DiVincenzo, D. P. The Physical Implementation of Quantum Computation. *Fortschr. Phys.* **2000**, *48*, 771−783.

(5) Kłos, J.; Kotochigova, S. Prospects for Laser Cooling of Polyatomic Molecules with Increasing Complexity. *Phys. Rev. Research* **2020**, *2*, 013384.

(6) Brazier, C.; Bernath, P. Laser and Fourier Transform Spectroscopy of the $\tilde{A}^2\Pi$-$\tilde{X}^2\Sigma^+$ Transition of SrOH. *J. Mol. Spectrosc.* **1985**, *114*, 163−173.

(7) Brazier, C.; Ellingboe, L.; Kinsey-Nielsen, S.; Bernath, P. Laser Spectroscopy of Alkaline Earth Monoalkoxide Free Radicals. *J. Am. Chem. Soc.* **1986**, *108*, 2126−2132.

(8) Ortiz, J. Ground and Excited States of CaCH3, CaNH2, CaOH, and CaF through Electron Propagator Calculations. *J. Chem. Phys.* **1990**, *92*, 6728−6731.

(9) Ortiz, J. Ground and Excited States of CaSH through Electron Propagator Calculations. *Chem. Phys. Lett.* **1990**, *169*, 116−120.

(10) Augenbraun, B. L.; Lasner, Z. D.; Frenett, A.; Sawaoka, H.; Miller, C.; Steimle, T. C.; Doyle, J. M. Laser-cooled Polyatomic Molecules for Improved Electron Electric Dipole Moment Searches. *New J. Phys.* **2020**, *22*, 022003.

(11) Wormsbecher, R.; Suenram, R. Laser Spectroscopy and Chemiluminescence from the Monomethoxides of Ca, Sr, and Ba. *J. Mol. Spectrosc.* **1982**, *95*, 391−404.

(12) O'Brien, L.; Brazier, C.; Bernath, P. High-resolution Laser Spectroscopy of Strontium Monomethoxide, SrOCH3. *J. Mol. Spectrosc.* **1988**, *130*, 33−45.

(13) Crozet, P.; Martin, F.; Ross, A.; Linton, C.; Dick, M.; Adam, A. The A2E−X2A1 System of CaOCH3. *J. Mol. Spectrosc.* **2002**, *213*, 28−34.

(14) Forthomme, D.; Linton, C.; Read, A.; Tokaryk, D.; Adam, A.; Downie, L.; Granger, A.; Hopkins, W. Unravelling the Visible Spectrum of Strontium Monomethoxide. *J. Mol. Spectrosc.* **2011**, *270*, 108−115.

(15) Kozyryev, I.; Baum, L.; Matsuda, K.; Doyle, J. M. Proposal for Laser Cooling of Complex Polyatomic Molecules. *ChemPhysChem* **2016**, *17*, 3641−3648.

(16) Kozyryev, I.; Steimle, T. C.; Yu, P.; Nguyen, D.-T.; Doyle, J. M. Determination of CaOH and CaOCH3 vibrational branching ratios for direct laser cooling and trapping. *New J. Phys.* **2019**, *21*, 052002.

(17) Mitra, D.; Vilas, N. B.; Hallas, C.; Anderegg, L.; Augenbraun, B. L.; Baum, L.; Miller, C.; Raval, S.; Doyle, J. M. Direct Laser Cooling of a Symmetric Top Molecule. *Science* **2020**, *369*, 1366−1369.

(18) Augenbraun, B. L.; Lasner, Z. D.; Frenett, A.; Sawaoka, H.; Le, A. T.; Doyle, J. M.; Steimle, T. C. Observation and Laser Spectroscopy of Ytterbium Monomethoxide, YbOCH3. *Phys. Rev. A: At., Mol., Opt. Phys.* **2021**, *103*, 022814.

(19) Ivanov, M. V.; Bangerter, F. H.; Wójcik, P.; Krylov, A. I. Toward Ultracold Organic Chemistry: Prospects of Laser Cooling Large Organic Molecules. *J. Phys. Chem. Lett.* **2020**, *11*, 6670−6676.

(20) Dickerson, C. E.; Guo, H.; Shin, A. J.; Augenbraun, B. L.; Caram, J. R.; Campbell, W. C.; Alexandrova, A. N. Franck-Condon Tuning of Optical Cycling Centers by Organic Functionalization. *Phys. Rev. Lett.* **2021**, *126*, 123002.

(21) Snow, T. P.; Witt, A. N. The Interstellar Carbon Budget and the Role of Carbon in Dust and Large Molecules. *Science* **1995**, *270*, 1455−1460.

(22) Tielens, A. Interstellar Polycyclic Aromatic Hydrocarbon Molecules. *Annu. Rev. Astron. Astrophys.* **2008**, *46*, 289−337.

(23) Hardegree-Ullman, E.; Gudipati, M.; Boogert, A.; Lignell, H.; Allamandola, L. J.; Stapelfeldt, K. R.; Werner, M. *Astrophys. J.* **2014**, *784*, 172.

(24) Hanine, M.; Meng, Z.; Lu, S.; Xie, P.; Picaud, S.; Devel, M.; Wang, Z. Formation of Interstellar Complex Polycyclic Aromatic Hydrocarbons: Insights from Molecular Dynamics Simulations of Dehydrogenated Benzene. *Astrophys. J.* **2020**, *900*, 188.

(25) Young, E. T.; Becklin, E. E.; Marcum, P. M.; Roellig, T. L.; Buizer, J. M. D.; Herter, T. L.; Güsten, R.; Dunham, E. W.; Temi, P.; Andersson, B.-G.; et al. Early Science with SOFIA, the Stratospheric Observatory for Infrared Astronomy. *Astrophys. J., Lett.* **2012**, *749*, L17.

(26) Bauschlicher, C. W.; Boersma, C.; Ricca, A.; Mattioda, A. L.; Cami, J.; Peeters, E.; de Armas, F. S.; Saborido, G. P.; Hudgins, D. M.; Allamandola, L. J. The NASA Ames Polycyclic Aromatic Hydrocarbon Infrared Spectroscopic Database: The Computed Spectra. *Astrophys. J., Suppl. Ser.* **2010**, *189*, 341−351.

(27) Malloci, G.; Joblin, C.; Mulas, G. Online Database of the Spectral Properties of Polycyclic Aromatic Hydrocarbons. *Chem. Phys.* **2007**, *332*, 353−359.

(28) Ivanov, M. V.; Gulania, S.; Krylov, A. I. Two Cycling Centers in One Molecule: Communication by Through-Bond Interactions and Entanglement of the Unpaired Electrons. *J. Phys. Chem. Lett.* **2020**, *11*, 1297−1304.

(29) Berlman, I. *Handbook of Fluorescence Spectra of Aromatic Molecules*; Academic Press, 1971.

(30) Smyth, K. C.; Schiavone, J. A.; Freund, R. S. Excitation of Fluorescence in Naphthalene and Azulene by Electron Impact. *J. Chem. Phys.* **1975**, *62*, 136−144.

(31) Novak, J.; Windsor, M. Laser Photolysis and Spectroscopy in the Nanosecond Time Range: Excited Singlet State Absorption in Coronene. *J. Chem. Phys.* **1967**, *47*, 3075−3076.

(32) Augenbraun, B. L.; Doyle, J. M.; Zelevinsky, T.; Kozyryev, I. Molecular Asymmetry and Optical Cycling: Laser Cooling Asymmetric Top Molecules. *Phys. Rev. X* **2020**, *10*, 031022.

(33) Guo, H.; Dickerson, C. E.; Shin, A. J.; Zhao, C.; Atallah, T. L.; Caram, J. R.; Campbell, W. C.; Alexandrova, A. N. Surface Chemical Trapping of Optical Cycling Centers. *Phys. Chem. Chem. Phys.* **2021**, *23*, 211−218.

(34) Ellis, A. M. Main Group Metal-Ligand Interactions in Small Molecules: New Insights from Laser Spectroscopy. *Int. Rev. Phys. Chem.* **2001**, *20*, 551−590.

(35) Piskorski, J.; Patterson, D.; Eibenberger, S.; Doyle, J. M. Cooling, Spectroscopy and Non-Sticking of trans-Stilbene and Nile Red. *ChemPhysChem* **2014**, *15*, 3800−3804.

(36) Patterson, D.; Tsikata, E.; Doyle, J. M. Cooling and Collisions of Large Gas Phase Molecules. *Phys. Chem. Chem. Phys.* **2010**, *12*, 9736−9741.

(37) Perdew, J. P.; Ernzerhof, M.; Burke, K. Rationale for Mixing Exact Exchange with Density Functional Approximations. *J. Chem. Phys.* **1996**, *105*, 9982−9985.

(38) Grimme, S.; Anthony, J.; Ehrlich, S.; Krieg, H. A Consistent and Accurate Ab Initio Parametrization of Density Functional Dispersion Correction (DFT-D) for the 94 Elements H-Pu. *J. Chem. Phys.* **2010**, *132*, 154104.

(39) Rappoport, D.; Furche, F. Property-optimized Gaussian Basis Sets for Molecular Response Calculations. *J. Chem. Phys.* **2010**, *133*, 134105.

(40) Frisch, M. J.; Trucks, G. W.; Schlegel, H. B.; Scuseria, G. E.; Robb, M. A.; Cheeseman, J. R.; Scalmani, G.; Barone, V.; Petersson, G. A.; Nakatsuji, H. et al. *Gaussian 16*, Revision C.01; Gaussian Inc.: Wallingford, CT, 2016.

(41) Cané, E.; Miani, A.; Trombetti, A. Anharmonic Force Fields of Naphthalene-h 8 and Naphthalene-d 8. *J. Phys. Chem. A* **2007**, *111*, 8218−8222.

(42) Mackie, C. J.; Candian, A.; Huang, X.; Maltseva, E.; Petrignani, A.; Oomens, J.; Buma, W. J.; Lee, T. J.; Tielens, A. G. G. M. The Anharmonic Quartic Force Field Infrared Spectra of Three Polycyclic

https://doi.org/10.1021/acs.jpclett.1c00733
J. Phys. Chem. Lett. 2021, 12, 3989−3995

Aromatic Hydrocarbons: Naphthalene, Anthracene, and Tetracene. *J. Chem. Phys.* **2015**, *143*, 224314.
(43) Lu, T.; Chen, F. Multiwfn: A multifunctional wavefunction analyzer. *J. Comput. Chem.* **2012**, *33*, 580−592.
(44) Kresse, G.; Furthmüller, J. Efficient Iterative Schemes for Ab Initio Total-Energy Calculations Using a Plane-Wave Basis Set. *Phys. Rev. B: Condens. Matter Mater. Phys.* **1996**, *54*, 11169−11186.
(45) Kresse, G.; Furthmüller, J. Efficiency of Ab-initio Total Energy Calculations for Metals and Semiconductors Using a Plane-Wave Basis Set. *Comput. Mater. Sci.* **1996**, *6*, 15−50.
(46) Kresse, G.; Hafner, J. Ab Initio Molecular-Dynamics Simulation of the Liquid-Metal−Amorphous-Semiconductor Transition in Germanium. *Phys. Rev. B: Condens. Matter Mater. Phys.* **1994**, *49*, 14251−14269.
(47) Kresse, G.; Hafner, J. Ab Initio Molecular Dynamics for Liquid Metals. *Phys. Rev. B: Condens. Matter Mater. Phys.* **1993**, *47*, 558−561.
(48) Perdew, J. P.; Burke, K.; Ernzerhof, M. Generalized Gradient Approximation Made Simple. *Phys. Rev. Lett.* **1997**, *78*, 1396.
(49) Perdew, J. P.; Burke, K.; Ernzerhof, M. Generalized Gradient Approximation Made Simple. *Phys. Rev. Lett.* **1996**, *77*, 3865−3868.
(50) Krukau, A. V.; Vydrov, O. A.; Izmaylov, A. F.; Scuseria, G. E. Influence of the Exchange Screening Parameter on the Performance of Screened Hybrid Functionals. *J. Chem. Phys.* **2006**, *125*, 224106.
(51) Tang, W.; Sanville, E.; Henkelman, G. A Grid-based Bader Analysis Algorithm Without Lattice Bias. *J. Phys.: Condens. Matter* **2009**, *21*, 084204.
(52) Henkelman, G.; Arnaldsson, A.; Jónsson, H. A Fast and Robust Algorithm for Bader Decomposition of Charge Density. *Comput. Mater. Sci.* **2006**, *36*, 354−360.
(53) Borlido, P.; Aull, T.; Huran, A.; Tran, F.; Marques, M. A. L.; Botti, S. *J. Chem. Theory Comput.* **2019**, *15*, 5069−5079.
(54) Borlido, P.; Schmidt, J.; Huran, A. W.; Tran, F.; Marques, M. A. L.; Botti, S. Exchange-correlation functionals for band gaps of solids: benchmark, reparametrization and machine learning. *npj Comput. Mater.* **2020**, *6*, 96.
(55) Kresse, G.; Joubert, D. From Ultrasoft Pseudopotentials to the Projector Augmented-Wave Method. *Phys. Rev. B: Condens. Matter Mater. Phys.* **1999**, *59*, 1758−1775.
(56) Blöchl, P. E. Projector Augmented-Wave Method. *Phys. Rev. B: Condens. Matter Mater. Phys.* **1994**, *50*, 17953−17979.

■ NOTE ADDED AFTER ASAP PUBLICATION

This paper was published ASAP on April 20, 2021, with an earlier draft of the Supporting Information file. The corrected version was posted on April 29, 2021.

https://doi.org/10.1021/acs.jpclett.1c00733
J. Phys. Chem. Lett. 2021, 12, 3989−3995